

# Structure of the $\alpha_2\varepsilon_2$ Ni-dependent CO dehydrogenase component of the *Methanosarcina barkeri* acetyl-CoA decarbonylase/synthase complex

Weimin Gong<sup>†‡§</sup>, Bing Hao<sup>§¶</sup>, Zhiyi Wei<sup>†‡</sup>, Donald J. Ferguson, Jr.<sup>||</sup>, Thomas Tallant<sup>||</sup>, Joseph A. Krzycki<sup>||†‡‡‡</sup>, and Michael K. Chan<sup>||†‡‡‡§§</sup>

Departments of <sup>¶</sup>Biochemistry, <sup>§§</sup>Chemistry and <sup>||</sup>Microbiology, and <sup>††</sup>Ohio State Biochemistry Program, Ohio State University, 484 West 12th Avenue, Columbus, OH 43210; <sup>†</sup>National Laboratory of Biomacromolecules, Institute of Biophysics, Chinese Academy of Sciences, Beijing 100101, People's Republic of China; and <sup>‡</sup>School of Life Sciences, University of Science and Technology of China, Hefei, Anhui 230026, People's Republic of China

Edited by Harry B. Gray, California Institute of Technology, Pasadena, CA, and approved April 21, 2008 (received for review January 15, 2008)

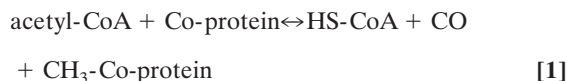
Ni-dependent carbon monoxide dehydrogenases (Ni-CODHs) are a diverse family of enzymes that catalyze reversible CO:CO<sub>2</sub> oxidoreductase activity in acetogens, methanogens, and some CO-using bacteria. Crystallography of Ni-CODHs from CO-using bacteria and acetogens has revealed the overall fold of the Ni-CODH core and has suggested structures for the C cluster that mediates CO:CO<sub>2</sub> interconversion. Despite these advances, the mechanism of CO oxidation has remained elusive. Herein, we report the structure of a distinct class of Ni-CODH from methanogenic archaea: the  $\alpha_2\varepsilon_2$  component from the  $\alpha_8\beta_8\gamma_8\delta_8\varepsilon_8$  CODH/acetyl-CoA decarbonylase/synthase complex, an enzyme responsible for the majority of biogenic methane production on Earth. The structure of this Ni-CODH component provides support for a hitherto unobserved state in which both CO and H<sub>2</sub>O/OH<sup>-</sup> bind to the Ni and the exogenous FCII iron of the C cluster, respectively, and offers insight into the structures and functional roles of the  $\varepsilon$ -subunit and FeS domain not present in nonmethanogenic Ni-CODHs.

carbon dioxide | carbon monoxide | oxidoreductase | acetate | methanogenesis

Increasing levels of atmospheric methane and carbon dioxide are thought to greatly influence global warming, a phenomenon dramatically impacting ecosystems worldwide. Although most of the concern has been on human activities, natural sources also serve as major contributors to the levels of these gases. Thus, detailed understanding of the responsible biological pathways is of significance.

One such process is methanogenesis from acetic acid (CH<sub>3</sub>COOH → CO<sub>2</sub> + CH<sub>4</sub>), which produces two-thirds of methane originating from natural sources (1). The central enzyme in this pathway is acetyl-CoA decarbonylase/synthase (ACDS), a multimeric 2.4-MDa  $\alpha_8\beta_8\gamma_8\delta_8\varepsilon_8$  complex that mediates multiple reactions (2, 3). In *Methanosarcina barkeri*, the  $\alpha$  to  $\varepsilon$  subunits have sizes of 89, 60, 50, 48, and 20 kDa, respectively (4, 5). The fundamental activities of the ACDS complex are:

Acetyl-CoA synthase activity:



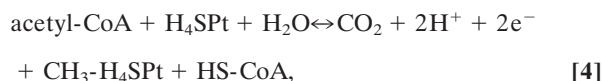
Co- $\beta$ -Me-cobamide:tetrahydropterin methyltransferase activity:



CO:CO<sub>2</sub> oxidoreductase activity:



and net reaction:



where H<sub>4</sub>Spt, tetrahydrosarcinapterin; CH<sub>3</sub>-H<sub>4</sub>Spt, methyl-tetrahydrosarcinapterin; and Co-protein (corrinoid-protein), the corrinoid/iron sulfur component formed from the  $\gamma$ - and  $\delta$ -subunits. An important feature of these reactions is their reversibility. Indeed, although methanogenesis involves the consumption of acetate, genetic and biochemical studies have shown the ability of methanogens to produce acetate (as acetyl-CoA) by reverse reaction-mimicking the Ljungdahl-Wood pathway of acetogens (6).

CO dehydrogenase (CODH) activity is associated with the  $\alpha$ - and  $\varepsilon$ -subunits that can be isolated as a 220-kDa  $\alpha_2\varepsilon_2$  component (7). The  $\alpha$ -subunit exhibits partial sequence homology to the Ni-CODH enzymes from CO-using bacteria and the Ni-CODH domain of acetogenic CODH/ACS enzymes, all of which use a catalytic NiFe<sub>4</sub>S<sub>4</sub>-containing C-cluster to mediate the reversible CODH chemistry (8–13). The role of the  $\varepsilon$ -subunit, however, has been unknown, because it does not evince homology with acetogenic CODH/ACS. However, a role in stabilization of the  $\alpha_2\varepsilon_2$  was suggested (14).

Acetyl-CoA synthase (ACS) activity is associated with the  $\beta$ -subunit (4). Both truncated  $\beta^*$  subunit generated with chymotrypsin (4) and recombinant  $\beta$  subunit (15) exhibit high acetyltransferase activity, as assayed by monitoring acetyl group transfer from acetyl-CoA to 3'-dephospho-CoA (4, 16). Additional support for this assignment comes from the structures of synthase domains of the *Morella thermoacetica* CODH/ACS and *Carboxydotherrmus hydrogenoformans* ACS (10, 11). The ACS domain of these proteins contains the A center and shares homology with the  $\beta$ -subunit of the ACDS complex, suggesting a similar role.

The CH<sub>3</sub>-H<sub>4</sub>Spt:corrinoid methyltransferase activity of the ACDS is localized to the  $\gamma\delta$  subunits, which can be separated from the full ACDS complex with cationic detergent (17) or by proteolysis (4). Potential insight into the 3D structure of these subunits of the methanogen ACDS complex has recently been

Author contributions: B.H., J.A.K., and M.K.C. designed research; W.G., B.H., Z.W., D.J.F., T.T., and M.K.C. performed research; W.G., B.H., Z.W., J.A.K., and M.K.C. analyzed data; and W.G., B.H., J.A.K., and M.K.C. wrote the paper.

The authors declare no conflict of interest.

This article is a PNAS Direct Submission.

Data deposition: The coordinates have been deposited in the Protein Data Bank (PDB ID code 3CF4).

§W.G. and B.H. contributed equally to this work.

\*\*To whom correspondence may be addressed. E-mail: krzycki.1@osu.edu or chan@chemistry.ohio-state.edu.

This article contains supporting information online at [www.pnas.org/cgi/content/full/0800415105/DCSupplemental](http://www.pnas.org/cgi/content/full/0800415105/DCSupplemental).

© 2008 by The National Academy of Sciences of the USA

provided by the structure of the corrinoid iron–sulfur protein involved in acetyl-CoA synthesis in *C. hydrogenoformans* (18).

Although the components of the methanogenic ACDS complex exhibit homology to proteins structurally characterized from acetogens and CO<sub>2</sub>-using bacteria, no crystal structures of the proteins or components of the methanogenic ACDS complex have been determined. Thus, no structural information exists for a distinctive class of CODH enzymes responsible for methanogenesis from acetate, the predominant methane precursor in many environments. Toward elucidating their features and unique properties, we have undertaken the structural determination of each of the functional components of the ACDS complex isolated from a methanogen grown on acetate as sole source of methane and reducing power, with the goal of constructing a model for the entire protein. Herein, we describe the structure of the first of these targets, the  $\alpha_2\epsilon_2$  CO dehydrogenase component [class I CODH/ACDS (19)] from *M. barkeri* and compare it with the determined structures, namely the Ni-dependent CODH/ACS (class III) from the acetogen *M. thermoacetica* (10, 11) and the Ni-CODH (class IV) from the phototrophic bacteria *C. hydrogenoformans* (8) and *Rhodospirillum rubrum* (9). These related Ni-CODHs have been shown to share a similar active site but exhibit significant differences in their global sequence and overall oligomerization. The structure of the C cluster in the *M. barkeri* Ni-CODH was analyzed and provides the visualization of a CODH with both CO and H<sub>2</sub>O bound to the enzyme. Notably, analysis of the additional regions in the *M. barkeri* Ni-CODH leads us to suggest alternate pathways for electron transfer and substrate channeling not observed in the previous acetogenic CODH/ACS and other Ni-CODH structures, possibly reflecting the distinct role the *M. barkeri* enzyme plays in aceticlastic methanogenesis.

## Results

**Overall Structure.** The Ni-CODH component of the *M. barkeri* ACDS complex crystallizes as a  $\alpha_2\epsilon_2$  oligomer, consistent with the biochemical data (7) (Fig. 1). Although the asymmetric unit contains only one  $\alpha\epsilon$  heterodimer, a crystallographic twofold axis lies between adjacent  $\alpha$ -subunits generating the observed  $\alpha_2\epsilon_2$  oligomer. This arrangement is distinct from that predicted for the 26-Å EM structure of the  $\alpha_2\epsilon_2$  complex from *M. thermophila* (14) but is similar to that of related crystal structures of Ni-CODHs from nonmethanogens (8–11).

The two  $\alpha$ -subunits form the core of the  $\alpha_2\epsilon_2$  oligomer and exhibit extensive interaction (Fig. 1 *A* and *C*), burying a total of  $\approx 7,300$  Å<sup>2</sup> of solvent accessible surface area between them. The  $\epsilon$ -subunits lie away from the crystallographic twofold axis and interact primarily with one  $\alpha$ -subunit, although one loop (residues 11–17) extends out to interact with both the  $\alpha$ - and  $\epsilon$ -subunits of the twofold related heterodimer. The interaction between the  $\alpha$ - and  $\epsilon$ -subunits is stabilized by hydrophobic interactions and hydrogen bonds and appears fairly tight (Fig. 1 *A* and *F*), burying  $\approx 3,700$  Å<sup>2</sup> of solvent accessible surface area.

Each  $\alpha\epsilon$  heterodimer contains five iron–sulfur clusters localized to the  $\alpha$ -subunit, two Fe<sub>4</sub>S<sub>4</sub> clusters (B and D clusters) and one Ni-Fe-S cluster (C cluster) observed in other Ni-CODH structures, and two Fe<sub>4</sub>S<sub>4</sub> clusters not observed in other Ni-CODH structures and that are designated the E and F clusters (12). Because the D cluster lies along the twofold axis, the overall  $\alpha_2\epsilon_2$  complex contains nine metal clusters arranged as shown in Fig. 1*B*. The arrangement of the B, C, and D clusters is similar to that observed in other Ni-CODH enzymes. One important difference, however, is that, whereas in the previous Ni-CODH structures the D cluster was fairly accessible, lying near the surface of the protein, in the *M. barkeri* Ni-CODH structure, access to the D cluster is much more restricted because of the placement of the  $\epsilon$ -subunits.

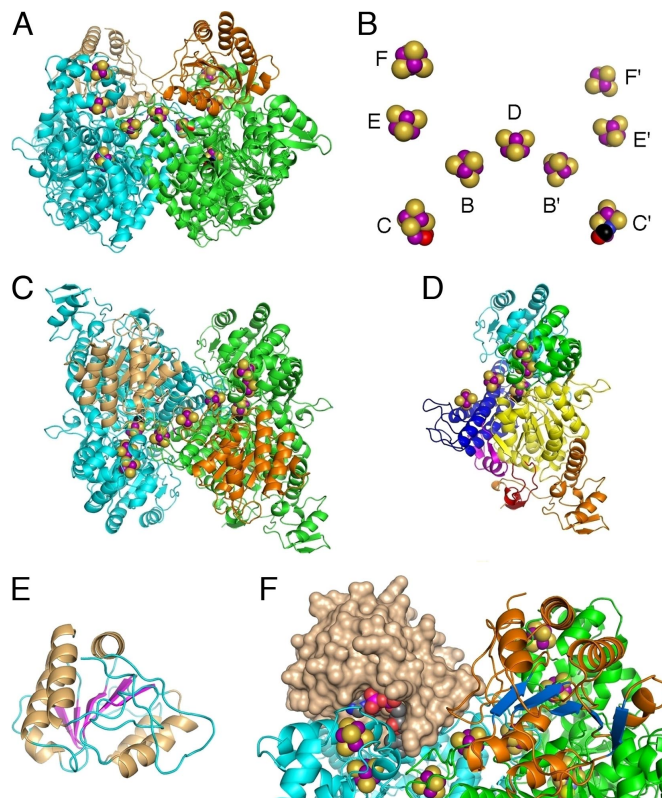


**Fig. 1.** The *M. barkeri*  $\alpha_2\epsilon_2$  Ni-CODH component, subunits, and cofactors. (*A*) Side view of the  $\alpha_2\epsilon_2$  component. The protein is shown as ribbons with the  $\alpha$ -subunits colored in cyan and green and the  $\epsilon$ -subunits in tan and orange. The atoms of the metal clusters are shown as spheres, with Fe atoms colored in purple, Ni atoms in blue, and the remaining atoms in CPK. (*B*) Side view of metal clusters in the  $\alpha_2\epsilon_2$  complex. (*C*) Top view of the  $\alpha_2\epsilon_2$  component. (*D*) Top view of the right  $\alpha$ -subunit highlighting its different domains. The  $\epsilon$ -subunit is omitted. The  $\alpha$ -subunit is colored in rainbow by domain: N-terminal portion (magenta), N-terminal  $\alpha$ -helical domain (blue), first Rossmann-like domain (cyan), FeS-binding domain (green), second C-cluster Rossmann-like domain (yellow), and C-terminal domain (orange). The  $\beta$ -hairpin insert in the second Rossmann-like domain is colored in red. (*E*) Ribbon diagram of  $\epsilon$ -subunit colored by secondary structure with  $\alpha$ -helices in tan,  $\beta$ -sheets in magenta, and loops in cyan. The orientation of this subunit matches the  $\epsilon$ -subunit shown as tan surface in *F*. (*F*) Docking interaction between the  $\alpha$ - and  $\epsilon$ -subunits colored as in *A*. The left  $\epsilon$ -subunit is shown as a surface with an FAD molecule shown and colored in CPK to illustrate its fit to the cavity. No FAD was observed in the  $\alpha_2\epsilon_2$  structure. The  $\beta$ -strands in the right  $\epsilon$ -subunit are colored in marine for better visualization.

**The  $\alpha$ -Subunit.** The  $\alpha$ -subunit of the *M. barkeri* Ni-CODH component can be divided into two regions: a core region (residues 72–405, 487–806) found in all Ni-CODHs and an Fe<sub>4</sub>S<sub>4</sub>-binding domain (residues 406–486) found in only methanogenic and other class I/II CODH/ACS enzymes (19) (Fig. 1*D*). As described in structures of other Ni-CODHs, the core region is comprised of three domains: an N-terminal  $\alpha$ -helical domain (residues 72–221) that provides the Cys ligands to the B cluster (Cys-76, -79, -84, and -94) and D cluster (Cys-73 and -77) and two  $\alpha/\beta$  Rossmann-like domains (residues 222–404 and 487–717), which together provide the ligands for the C cluster (residues His-250, Cys-278, Cys-323, Cys-523, Cys-552, and Cys-587).

The general features of the core region of the  $\alpha$ -subunit are highly similar to that observed in other Ni-CODHs, with the exception of three specific regions: an N-terminal portion (residues 41–71), a  $\beta$ -hairpin (residues 667–693), and a C-terminal portion (residues 718–806) (Fig. 1*D*). A mapping of these regions reveals they all adopt positions corresponding to the CODH/ACS interface

in the structure of the *M. thermoacetica* CODH/ACS (10, 11). Although it might be initially tantalizing to speculate that these three regions mediate interactions with the  $\beta$ -subunit of ACDS complex in the same fashion as observed in the *M. thermoacetica* CODH/ACS, sequence analyses prevent this natural correlation. The key difference is that the *M. thermoacetica* ACS subunit contains an additional Rossmann-fold N-terminal domain absent in the  $\beta$ -subunit of the *M. barkeri* ACDS. Thus, the *M. barkeri* ACDS  $\beta$ -subunit must bind in a different manner.

The  $\text{Fe}_4\text{S}_4$ -binding domain of the  $\alpha$ -subunit is formed from six  $\alpha$ -helices and binds two  $\text{Fe}_4\text{S}_4$  clusters: an E cluster coordinated by residues Cys-427, -455, -458, and -461, and an F-cluster coordinated by residues Cys-417, -420, -423, and -465. All these Cys residues are highly conserved in class I/II CODH/ACDS enzymes (19). Structural alignments with DALI (20) reveal potential homology of this domain with the FeS domain of dihydropyrimidine dehydrogenase, whereas sequence alignments with PSI-BLAST and BLASTP (21) reveal sequence homology (34% identity) of a specific face of the FeS domain that wraps around the two FeS clusters (residues 411–439 and 448–465) with the  $\delta$ -subunit of methanogenic pyruvate oxidoreductases (POR).

**The  $\epsilon$ -Subunit.** The  $\epsilon$ -subunit of the *M. barkeri* Ni-CODH component adopts a Rossmann fold consisting of a central parallel  $\beta$ -sheet flanked by six  $\alpha$ -helices—four  $\alpha$ -helices on one side (side I) and two  $\alpha$ -helices on the other side (side II) (Fig. 1E). The two  $\alpha$ -helices on side II, the N-terminal loop, and several other short loops participate in forming the  $\alpha\epsilon$ -subunit interface (Fig. 1F). Structural and sequence alignments reveal that the  $\epsilon$ -subunit belongs to the DHS-like NAD/FAD-binding domain clan, whose most notable members are the middle domains found in a number of thiamine pyrophosphate (TPP)-dependent enzymes including the structurally characterized acetolactate synthase (22), pyruvate oxidase (23), and pyruvate decarboxylase (24). In these TPP enzymes, the middle domain generally serves as a role in binding dinucleotide cofactors (e.g., FAD/NAD) for dinucleotide-dependent regulation. To facilitate this role, these middle domains contain a site that specifically binds the adenine group of the dinucleotide cofactor. Notably, this binding site is conserved in the structural fold of the  $\epsilon$ -subunit.

**The C Cluster and the Environment of the Active Site.** Perhaps the site of greatest interest in structures of Ni-CODH enzymes is the C cluster, given its central role in mediating CO oxidation chemistry. Despite the publication and release of structures for several Ni-CODH enzymes, one major area of contention had been the presence/absence of a bridging sulfide group between the Ni and external Fe site. Although the first and highest-resolution *C. hydrogenoformans* Ni-CODH structure (8) clearly showed the presence of density consistent with a bridging sulfide ligand, none of the other Ni-CODH structures (9–11) exhibited similar evidence for such a group.

Based on their and other biochemical studies, Feng *et al.* (25) suggested that instead of a bridging sulfide, CO binds to the Ni and a bridging water/hydroxyl to the FCII iron. Structural support for this hypothesis has recently come from Jeong and Dobbek (26), who report the structures of the *C. hydrogenoformans* at three different states, including one that contains bound  $\text{CO}_2$ . Notably, the C clusters in these *C. hydrogenoformans* Ni-CODH structures have no bridging sulfide and instead harbor a bound  $\text{H}_2\text{O}/\text{OH}^-$  or, in the case of the  $\text{CO}_2$ -treated protein, a  $\text{CO}_2$  molecule that bridges the Ni and exogenous FCII iron with the carbon of  $\text{CO}_2$  binding the Ni atom.

The C cluster in the *M. barkeri* Ni-CODH component is located in the  $\alpha$ -subunit in essentially the same position in the homologous domains of the previous Ni-CODH structures. Its

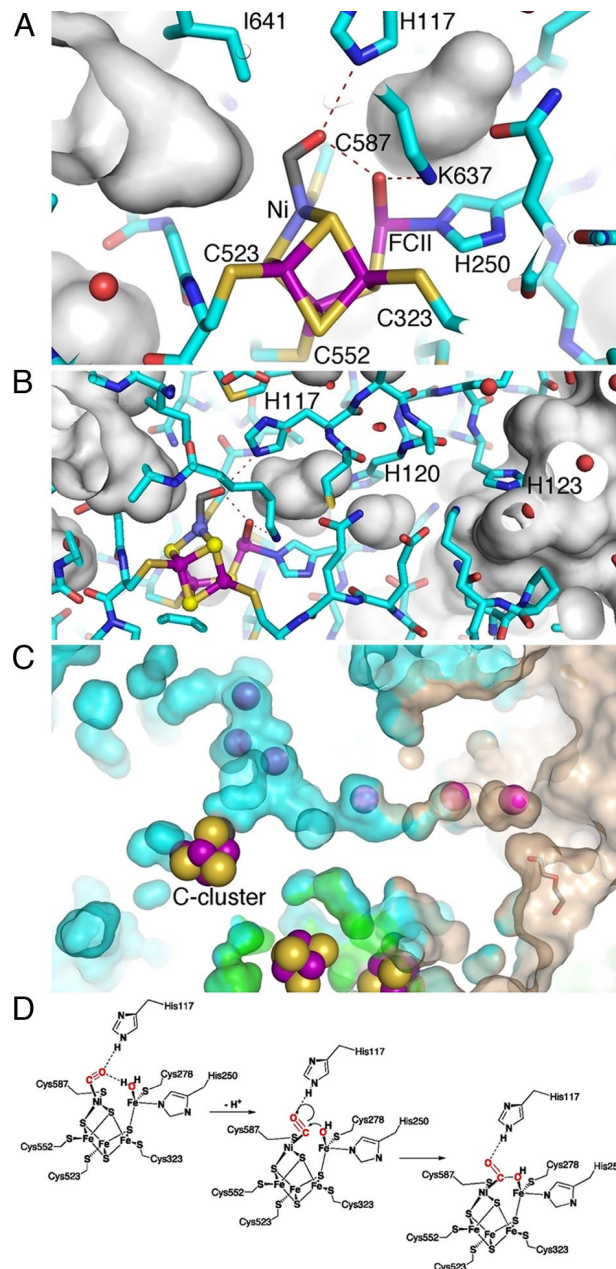


**Fig. 2.** Structure of the C cluster, putative substrate channels, and proposed mechanism of C-O bond formation. (A) Stick diagram of the C cluster and surrounding residues together with surface diagram highlighting internal cavities. The atoms of the C cluster including the bound CO and putative  $\text{H}_2\text{O}$  are colored by atom with Fe in violet, Ni in slate, carbon in gray, and sulfur in pink. The protein is shown in stick with the carbon atoms depicted in cyan and the remaining atoms in CPK. The Ni and FCII iron that bind CO and  $\text{H}_2\text{O}/\text{OH}^-$ , respectively, are labeled as are residues Ile-641 and His-117, which may help CO adopt its bent geometry. (B) Stick diagram highlighting putative proton/water channel. The conserved His residues that line one side of this channel are labeled. (C) The CO/ $\text{CO}_2$  channel of methanogenic CODH component depicted as a transparent molecular surface component colored by subunit according to the color scheme in Fig. 1. The protein atoms have been omitted for clarity, but the metal clusters are shown as spheres with Fe atoms colored in violet, Ni atoms in slate, and the remaining atoms in CPK. The Xe-binding sites that map the channel are shown as pink spheres. A small molecule modeled as a portion of a PEG group is shown in stick and colored in CPK. This PEG molecule marks the channel exit from the  $\epsilon$ -subunit. (D) Proposed coupling of the CO and  $\text{H}_2\text{O}$  species via intermediate observed in this structure. The loss of the proton required for  $\text{CO} + \text{OH}^-$  bond formation may account for the stability of the current intermediate, which was crystallized at low pH. All other Ni-CODH structures have been determined at neutral pH.

geometric arrangement [Fig. 2A and supporting information (SI) Fig. S1] is similar to that observed in the *R. rubrum* (9) and *M. thermoacetica* Ni-CODH structures, an NiFe<sub>4</sub>S<sub>4</sub> cluster comprised of a pseudocubane NiFe<sub>3</sub>S<sub>4</sub> cluster bridged to an exogenous Fe atom (Fe1), as opposed to the NiFe<sub>4</sub>S<sub>5</sub> cluster observed in the first and highest-resolution *C. hydrogenoformans* Ni-CODH structure. The protein ligands to the C cluster are conserved with those observed in all of the previous structures. Cysteine ligands Cys-323, -523, -552, and -587 bind Fe2, Fe3, Fe4, and Ni1 atoms of the NiFe<sub>4</sub>S<sub>4</sub> pseudocubane, respectively, whereas Cys-278 and His-250 serve as protein ligands to the exogenous iron (Fe1), also known as the FCII iron. A relatively conserved exogenous ligand, Cys-277, implicated in persulfide bridge formation (27), is located near but oriented away from the S3 sulfur of the C cluster.

Although the *M. barkeri* Ni-CODH C cluster lacks the additional  $\mu$ -S bridge observed in *C. hydrogenoformans* Ni-CODH structure, two additional peaks of electron density were found (Fig. S1). One peak could be fit to a monoatomic atom bound to the exogenous FCII iron. The other peak bound the Ni1 atom and could be best modeled as a diatomic ligand. The assignment of these exogenous ligands was made based on the magnitude of their electronic density and by noting their interactions with both the C cluster and noncoordinating residues near the C cluster active site, namely His-117 and Lys-637 (see Figs. S1–S3). These and several other noncoordinating residues, which are conserved in Ni-CODHs (12, 19), had been suggested to be involved in facilitating the reaction via acid base interactions (13). Using these criteria, the monoatomic atom bound to the FCII iron was assigned to a water/hydroxyl group based on its potential hydrogen-bonding interaction with the NZ atom of Lys-673 and the terminal atom of the exogenous diatomic ligand.

Following the same approach, the diatomic ligand was assigned to either a bent-terminal CO or bound formyl ligand. The assignment of the distant atom as oxygen was made based on potential hydrogen-bonding interactions with His-117 and the water/hydroxide bound to Fe1. The assignment of the more proximal atom as carbon was made based on the magnitude of its electron density and the absence of potential hydrogen-bonding interactions. A bound dioxygen ligand is unlikely, given the absence of hydrogen-bonding interaction with waters in the channel and the anaerobic crystallization conditions used to prevent FeS cluster degradation. This left CO and a formyl group as the most likely ligands at the site. Based on the bent geometry of the Ni-C-O bond, the more likely species might initially be considered a formyl group, given the much lower occurrence of bent metal carbonyls in biological systems. However, structural and sequence analyses of the ligands above the Ni sites reveal a conserved set of residues (Met-208, Thr-550, Asp-590, Ala-638, and Ile-641), whose positions suggest a potential steric hindrance that might induce the observed bent conformation. Modeling the bound diatomic group on the nickel as a linear CO leads to a potential steric clash based on the closer than van der Waals interaction of the CO oxygen with the CG1 carbon atom of the conformationally constrained Ile-641. Such a steric restriction could be functionally significant as inducing the CO ligand to adopt a bent conformation would reduce  $\pi$ -backbonding and help to lower the activation barrier for reversible CO oxidation.

Determining whether this steric hindrance is important to the CO oxidation mechanism will require biochemical studies of site-directed Ile-641 mutants. Nevertheless, the observed structural features of the *M. barkeri* C cluster, namely, (i) the binding of the diatomic ligand to Ni, (ii) the putative interaction of the carbonyl oxygen with His-117, and (iii) the steric constraints

identified by the bent carbonyl, may prove important in the C cluster-mediated reversible oxidation of CO.

**The Water and Gas Channels.** Previous structures of the *C. hydrogenoformans* Ni-CODH (8) and *M. thermoacetica* CODH/ACS (10, 11) revealed specific channels for CO/CO<sub>2</sub> and water. Given the internal location of the C cluster, these channels presumably facilitate the rapid exchange of substrates/products and, in the case of the *M. thermoacetica* CODH/ACS, to transport CO to the A center.

Previous analysis of the Ni-CODH structure from *C. hydrogenoformans* (8) led to the suggestion of a water channel near the B and D clusters. However, in the *M. barkeri* CODH structure, this channel is blocked by Tyr-661, a residue that is conserved in other class I/II CODH/ACS enzymes (19) and partially covered because of the location of the  $\epsilon$ -subunit. It appears more likely that the channel implicated in proton transfer in previous CODH structures (9, 12) also serves as the primary water channel in the methanogenic *M. barkeri* CODH. This proton channel (Fig. 2B), lined by three conserved histidine residues (His-117, -120, and -123), would be functionally advantageous as the water channel as well, because it provides a direct route from the protein surface to the FCII site proposed to bind H<sub>2</sub>O/OH. Consistent with this hypothesis, several water molecules are found in this region, and no salt bridges were identified. The only potential steric hindrance is a conserved histidine, His-120, which forms hydrogen bonds to two water molecules in the channel. The position of His-120 could allow it to shift and rotate in the channel depending on the positions of the water atoms and thereby regulate the flow of waters through the channel while hindering the escape of CO and CO<sub>2</sub> from the active site. A subsequent analysis revealed these features are shared by the *M. thermoacetica* CODH/ACS (10, 11) structures, suggesting this may be general water channel in multifunctional CODH/ACS enzymes. It is less likely that *C. hydrogenoformans* CODH utilizes this pathway, because a tyrosine and a histidine adopt positions over the channel (8) with side-chain positions stabilized by hydrogen-bonding interactions in that enzyme. One possible origin for the difference in CODH/ACS and CODH enzymes may be that *C. hydrogenoformans* CODH need not direct the CO and H<sub>2</sub>O water molecules along different pathways.

As in the previous structures, the *M. barkeri* CODH structure reveals an extended gas channel that passes by the C cluster and heads toward the opposite side of the C cluster-binding Rossmann domain (Fig. 2C). The channel appears tighter than in the previous structures, based on poorer connections between the interior solvent surface pockets, particularly near the surface of the protein. The identification of the primary hydrophobic gas-binding regions could be made by soaking *M. barkeri* CODH crystals with Xe and identifying the gas-binding sites in the interior of the protein. The combination of these gas-binding sites and interior surface map provides a clear picture of the middle part of the gas channel. The channel appears to take two pathways from the C cluster, with one pathway leading to the surface of the protein in the direction that may lead to the A center, whereas the other leads to and through the  $\epsilon$ -subunit. The side of the channel bordering the  $\epsilon$ -subunit also appears to have two secondary exits. One of these alternate exits is a water-filled channel near the surface of the  $\alpha$ -subunit, which is partially blocked by Ser-658, whereas the other opens into a large groove between the  $\alpha$ - and  $\epsilon$ -subunits but appears blocked by Thr-697.

## Discussion

**Proposed Role of the  $\epsilon$ -Subunit.** One intriguing question was whether the structure of the *M. barkeri* Ni-CODH might shed light on the role of the  $\epsilon$ -subunit, the subunit unique to class I/II Ni-CODHs. Previous biochemical studies noted that  $\epsilon_2$  dimers

were detectable in solution and therefore hypothesized that the  $\epsilon$ -subunit might act to stabilize the  $\alpha_2\epsilon_2$  complex (14). However, the *M. barkeri* Ni-CODH structure reveals few interactions between the two  $\epsilon$ -subunits that might suggest such a stabilizing role within the  $\alpha_2\epsilon_2$  component; an  $\epsilon$ - $\epsilon$  interaction between  $\alpha_2\epsilon_2$  units within the intact ACDS complex cannot be ruled out. We also considered the possibility that the  $\epsilon$ -subunit could serve as a gas channel to the A cluster within the  $\beta$ -subunit, noting that it served as one end of the channel adopted a Rossmann fold. Structure-based alignment of the ACS domain Rossmann with  $\epsilon$ -subunit resulted in a position for the A cluster that was far from the gas channel opening. This analysis led us to judge that a role as an interface to the  $\beta$ -subunit was unlikely.

However, our structural analysis suggests a hypothesis for the existence of the  $\epsilon$ -subunit in class I/II Ni-CODH proteins. Analysis of the structures of TPP middle domains reveals their common role in FAD and NAD binding (22–24). In these proteins, the TPP middle domain utilizes a conserved cavity to bind the adenine group of the FAD or NAD (see *SI Materials and Methods* and Fig. S4). Because this adenine cavity was conserved in the  $\epsilon$ -subunit, we explored this direction further by looking for a cavity of the appropriate size and distance to accommodate an FAD or NAD cofactor. Intriguingly, one such cavity was found. This cavity, formed between the interface of the  $\alpha$ - and  $\epsilon$ -subunits, is located near the D cluster, suggesting a plausible role in redox electron transfer. A subsequent survey of the literature revealed that FAD is a documented electron acceptor for the  $\alpha_2\epsilon_2$  component (5). Therefore, a plausible role for the  $\epsilon$ -subunit could be to provide the necessary binding sites required for FAD-mediated CO oxidation. Alternatively, binding of FAD or FADH<sub>2</sub> might regulate the activities of this major cellular oxidoreductase during autotrophic or acetotrophic conditions.

**Proposed Role of the FeS Domain.** Although FAD is one potential physiological electron acceptor of the *M. barkeri* Ni-CODH, the primary electron transfer partner of this enzyme and other Ni-CODH is ferredoxin. Based on the *R. rubrum*, *C. hydrogenoformans*, and *M. thermoaceticum* Ni-CODH structures, the likely pathway for electron transfer reactions between Ni-CODHs and ferredoxin in acetogens and CO using bacteria is through the D cluster. Presumably, ferredoxin becomes associated with a site near the D cluster, and electrons are transferred via an outer sphere mechanism. However, based on the *M. barkeri* Ni-CODH, this electron transfer pathway is unlikely in methanogenic Ni-CODHs, because the  $\epsilon$ -subunits are positioned over the D cluster, necessitating long electron transfer distances. Hence, we propose that the FeS domain in the  $\alpha$ -subunit, unique to class I/II Ni-CODHs, serves as the site of binding and electron transfer to ferredoxin.

This hypothesis is supported by a number of features, the most notable being the spatial locations of the unique Fe<sub>4</sub>S<sub>4</sub> clusters in the *M. barkeri* Ni-CODH structure. The positions of these E and F clusters are ideally situated to accept electrons from ferredoxin and then transfer these electrons to the B cluster, thereby accessing the common electron pathway used by other Ni-CODH enzymes. Other evidence comes from sequence analyses that reveal high sequence homology between one face of the FeS domain and the  $\delta$ -subunit of *M. barkeri* pyruvate ferredoxin oxidoreductase, which accepts electrons from ferredoxin to catalyze the couple of CO<sub>2</sub> and acetyl-CoA to produce pyruvate. Although unlikely to be a primary electron transfer pathway in methanogens, we note that the common binding of POR and methanogenic Ni-CODHs with ferredoxin provides a means to couple some of the electrons produced in CO oxidation with pyruvate synthesis. Such a pathway would be analogous to that proposed for the acetogen, *M. thermoacetica* (28).

Together with our analyses of the  $\epsilon$ -subunit, these data suggest

two distinct pathways for electron transfer between the C cluster and its physiological electron acceptor/donor. The C-B'-D pathway may be used for electron transfer to/from FAD, whereas the C-B'-E-F pathway is used for electron transfer to/from ferredoxin.

**Proposed Mechanism of Coupling in the Key C-O Forming Step.** There has been general support for the view that CO bound on Ni and OH<sup>-</sup> bound to the exogenous FCII iron are coupled to form CO<sub>2</sub> in the key C-O bond-forming step. The recent crystallographic studies of *C. hydrogenoformans* CODH appear to provide structures for the C cluster in states of the C cluster both preceding CO addition and after C-O bond formation. A key intermediate in the process of C-O bond formation missing from this series, however, is a structure of the C cluster in the state with bound CO and H<sub>2</sub>O. Our *M. barkeri* Ni-CODH, obtained at low pH, appears to fill this gap. With the caveat that the diatomic species identified bound to the Ni of the C cluster is CO, and not a formyl group, our work provides structural details for this CO-bound intermediate and suggests roles for Ile-641 and His-117 in helping to promote C-O bond formation. We note that the substrate carbonyl oxygen in both our CO-bound *M. barkeri* Ni-CODH and the recent CO<sub>2</sub>-bound *C. hydrogenoformans* Ni-CODH structures forms a hydrogen bond with His-117, but that the Ni ion adopts a different geometry switching from tetrahedral to more square planar configuration, respectively. These observations suggest the intriguing possibility that geometric changes in Ni could be linked to the CO<sub>2</sub> coupling chemistry (Fig. 2D).

## Conclusions

In summary, the structure of *M. barkeri* Ni-CODH component provides the structure of the third distinct class of Ni-CODH, one involved in an environmental process of global significance. The key findings of this work include the structural details of the  $\epsilon$ -subunit and FeS domain not present in other Ni-CODH proteins and their proposed roles in electron transfer to FAD and ferredoxin, respectively. Importantly, the methanogen enzyme also provides structural characterization of a C cluster intermediate that has both a bound CO and water. The structure of this intermediate provides support for coupling between a CO bound to Ni and a H<sub>2</sub>O/OH<sup>-</sup> bound to the exogenous FCII iron of the C cluster in the critical C-O bond forming step of Ni-CODHs.

## Methods

The detailed experimental procedures are provided in *SI Materials and Methods* and Table S1. In brief, the  $\alpha_2\epsilon_2$  Ni-CODH component of the *M. barkeri* ACDS complex was purified following established procedures (29). The protein was crystallized in an anaerobic chamber using 0.2 M (NH<sub>4</sub>)<sub>2</sub>SO<sub>4</sub>, 25% PEG 4K, and 0.1 M sodium acetate (pH 4.6) as the precipitant. Native Fe MAD datasets were collected on beamline X4A at the National Synchrotron Light Source, Brookhaven National Laboratory, Upton, NY (Table S1), whereas Xe-soaked crystals were prepared by using the MRC Cryo-Xe-Siter at the Stanford Synchrotron Radiation Laboratory (SSRL), Stanford, CA. The structure was determined by the multiple anomalous dispersion (MAD) method using two-wavelength Fe MAD data. The final model refined to an R factor of 20.9% and *R*<sub>free</sub> of 24.8%.

**ACKNOWLEDGMENTS.** M.K.C. dedicates this work to Prof. Mitsuru Kubota of Harvey Mudd College for introducing him to organometallic chemistry. We thank Dr. Craig Ogata for beamline assistance and Michael Soltis for assistance with the initial Xe-soaking experiments. X4A beamline at the National Synchrotron Light Source, a Department of Energy facility, is supported by the Howard Hughes Medical Institute. Work was done partially at SSRL, operated by the Department of Energy, Office of Basic Energy Sciences. This research was supported by National Institutes of Health Grant GM61796 and Department of Energy Grant DEFG0202-91ER200042. W.G. gratefully acknowledges support by Ministry of Science and Technology of China Grant 2006CB910903 and Natural Science Foundation of China Grant 30721003.

1. Ferry JG (1995) CO dehydrogenase. *Annu Rev Microbiol* 49:305–333.
2. Terlesky KC, Nelson MJ, Ferry JG (1986) Isolation of an enzyme complex with carbon monoxide dehydrogenase activity containing corrinoid and nickel from acetate-grown *Methanosarcina thermophila*. *J Bacteriol* 168:1053–1058.
3. Grahame DA (1991) Catalysis of acetyl-CoA cleavage and tetrahydrosarcinapterin methylation by a carbon monoxide dehydrogenase-corrinoid enzyme complex. *J Biol Chem* 266:22227–22233.
4. Grahame DA, DeMoll E (1996) Partial reactions catalyzed by protein components of the acetyl-CoA decarbonylase synthase enzyme complex from *Methanosarcina barkeri*. *J Biol Chem* 271:8352–8358.
5. Grahame DA, Stadtman TC (1987) Carbon monoxide dehydrogenase from *Methanosarcina barkeri*. Disaggregation, purification, and physicochemical properties of the enzyme. *J Biol Chem* 262:3706–3712.
6. Ladapo J, Whitman WB (1990) Method for isolation of auxotrophs in the methanogenic archaeobacteria: Role of the acetyl-CoA pathway of autotrophic CO<sub>2</sub> fixation in *Methanococcus marisaludis*. *Proc Natl Acad Sci USA* 87:5598–5602.
7. Krzycki JA, Zeikus JG (1984) Characterization and purification of carbon monoxide dehydrogenase from *Methanosarcina barkeri*. *J Bacteriol* 158:231–237.
8. Dobbek H, et al. (2001) Crystal structure of a carbon monoxide dehydrogenase reveals a [Ni-4Fe-5S] cluster. *Science* 293:1281–1285.
9. Drennan CL, et al. (2001) Life on carbon monoxide: X-ray structure of *Rhodospirillum rubrum* Ni-Fe-S carbon monoxide dehydrogenase. *Proc Natl Acad Sci USA* 98:11973–11978.
10. Doukov TI, et al. (2002) A Ni-Fe-Cu center in a bifunctional carbon monoxide dehydrogenase/acetyl-CoA synthase. *Science* 298:567–572.
11. Darnault C, et al. (2003) Ni-Zn-[Fe<sub>4</sub>-S<sub>4</sub>] and Ni-Ni-[Fe<sub>4</sub>-S<sub>4</sub>] clusters in closed and open subunits of acetyl-CoA synthase/carbon monoxide dehydrogenase. *Nat Struct Biol* 10:271–279.
12. Lindahl PA (2002) The Ni-containing carbon monoxide dehydrogenase family: light at the end of the tunnel? *Biochemistry* 41:2097–2105.
13. Ragsdale SW (2004) Life with carbon monoxide. *Crit Rev Biochem Mol Biol* 39:165–195.
14. Kocsis E, Kessel M, DeMoll E, Grahame DA (1999) Structure of the Ni/Fe-S protein subcomponent of the acetyl-CoA decarbonylase/synthase complex from *Methanosarcina thermophila* at 26-Å resolution. *J Struct Biol* 128:165–174.
15. Gencic S, Grahame DA (2003) Nickel in subunit beta of the acetyl-CoA decarbonylase/synthase multienzyme complex in methanogens. Catalytic properties and evidence for a binuclear Ni-Ni site. *J Biol Chem* 278:6101–6110.
16. Arndt JW, et al. (2004) Support for nickel as the labile metal in the A-center of the *M. barkeri* acetyl-CoA decarbonylase/synthase complex. *J Chin Chem Soc* 51:1253–1258.
17. Abbanat DR, Ferry JG (1991) Resolution of component proteins in an enzyme complex from *Methanosarcina thermophila* catalyzing the synthesis or cleavage of acetyl-CoA. *Proc Natl Acad Sci USA* 88:3272–3276.
18. Svetlitchnaia T, Svetlitchnyi V, Meyer O, Dobbek H (2006) Structural insights into methyltransfer reactions of a corrinoid iron-sulfur protein involved in acetyl-CoA synthesis. *Proc Natl Acad Sci USA* 103:14331–14336.
19. Lindahl PA, Chang B (2001) The evolution of acetyl-CoA synthase. *Orig Life Evol Biosph* 31:403–434.
20. Holm L, Sander C (1998) Touring protein fold space with Dali/FSSP. *Nucleic Acids Res* 26:316–319.
21. Altschul SF, et al. (1997) Gapped BLAST and PSI-BLAST: a new generation of protein database search programs. *Nucleic Acids Res* 25:3389–3402.
22. Pang SS, Duggleby RG, Schowen RL, Guddat LW (2004) The crystal structures of *Klebsiella pneumoniae* acetolactate synthase with enzyme-bound cofactor and with an unusual intermediate. *J Biol Chem* 279:2242–2253.
23. Muller YA, Schumacher G, Rudolph R, Schulz GE (1994) The refined structures of a stabilized mutant and of wild-type pyruvate oxidase from *Lactobacillus plantarum*. *J Mol Biol* 237:315–335.
24. Muller YA, Schulz GE (1993) Structure of the thiamine- and flavin-dependent enzyme pyruvate oxidase. *Science* 259:965–967.
25. Feng J, Lindahl PA (2004) Effect of sodium sulfide on Ni-containing carbon monoxide dehydrogenases. *J Am Chem Soc* 126:9094–9100.
26. Jeoung JH, Dobbek H (2007) Carbon dioxide activation at the Ni,Fe-cluster of anaerobic carbon monoxide dehydrogenase. *Science* 318:1461–1464.
27. Kim EJ, Feng J, Bramlett MR, Lindahl PA (2004) Evidence for a proton transfer network and a required persulfide-bond-forming cysteine residue in Ni-containing carbon monoxide dehydrogenases. *Biochemistry* 43:5728–5734.
28. Furdui C, Ragsdale SW (2000) The role of pyruvate ferredoxin oxidoreductase in pyruvate synthesis during autotrophic growth by the Wood-Ljungdahl pathway. *J Biol Chem* 275:28494–28499.
29. Krzycki JA, Mortenson LE, Prince RC (1989) Paramagnetic centers of carbon monoxide dehydrogenase from acetoclastic *Methanosarcina barkeri*. *J Biol Chem* 264:7217–7221.